

# Adiabatic mixed-field orientation of ground-state-selected carbonyl sulfide molecules

Jens S. Kienitz,<sup>1,2</sup> Sebastian Trippel,<sup>1,2, a)</sup> Terry Mullins,<sup>1</sup> Karol Długołęcki,<sup>1</sup> Rosario González-Férez,<sup>3, b)</sup> and Jochen Küpper<sup>1, 2, 4, c)</sup>

<sup>1)</sup> *Center for Free-Electron Laser Science (CFEL), Deutsches Elektronen-Synchrotron DESY, Notkestrasse 85, 22607 Hamburg, Germany*

<sup>2)</sup> *The Hamburg Center for Ultrafast Imaging, University of Hamburg, Luruper Chaussee 149, 22761 Hamburg, Germany*

<sup>3)</sup> *Instituto Carlos I de Física Teórica y Computacional and Departamento de Física Atómica, Molecular y Nuclear, Universidad de Granada, 18071 Granada, Spain*

<sup>4)</sup> *Department of Physics, University of Hamburg, Luruper Chaussee 149, 22761 Hamburg, Germany*

(Dated: 6 November 2018)

We experimentally demonstrated strong adiabatic mixed-field orientation  $N_{\text{up}}/N_{\text{tot}} = 0.882$  of carbonyl sulfide molecules (OCS) in their absolute ground state. OCS was oriented in combined non-resonant laser and static electric fields inside a two-plate velocity map imaging spectrometer. The transition from non-adiabatic to adiabatic orientation for the rotational ground state was studied by varying the applied laser and static electric field. Above static electric field strengths of 10 kV/cm and laser intensities of  $10^{11}$  W/cm<sup>2</sup> the observed degree of orientation reached a plateau. These results are in good agreement with computational solutions of the time-dependent Schrödinger equation.

PACS numbers: 37.10.-x, 37.10.Vz, 82.20.Bc

## I. INTRODUCTION

Molecular samples with directional order, e. g., oriented molecules, enable the extraction of information directly in the molecular frame, for instance, from photoelectron angular distributions,<sup>1–5</sup> high-order harmonic generation,<sup>6–8</sup> electron and x-ray diffractive imaging,<sup>9–11</sup> and stereochemistry experiments.<sup>12–14</sup> For diffraction experiments, data has often to be recorded and averaged over many shots. If the molecules in an ensemble have directional order, a molecular-frame diffraction pattern corresponding to the single-molecule signal above noise can be obtained.<sup>15–17</sup>

Various approaches have been developed to generate oriented molecules, including brute-force orientation using strong dc electric<sup>13,18,19</sup> and magnetic<sup>20</sup> fields, shaped<sup>21,22</sup> and two-color<sup>8,23,24</sup> near-infrared laser pulses, terahertz pulses,<sup>25–28</sup> multi-pulse schemes,<sup>8,28</sup> and mixed laser and dc electric field orientation.<sup>21,29–32</sup> In mixed-field orientation, the non-resonant laser field creates near degenerate doublets that are efficiently oriented by the dc electric field.<sup>29,30</sup> However, for the two components of the doublet the dipole moments, and thus the molecules, point in opposite directions, resulting in a reduced or vanishing macroscopic orientation depending on the populations of the two components.<sup>31</sup> Quantum-state selection allows for the preparation of ensembles of molecules all in a single rovibronic state.<sup>33–37</sup> Strong orientation can be achieved if these populations can be adiabatically transferred to the oriented field-dressed states. According to

the adiabaticity theorem,<sup>38</sup> the field-dressed dynamics are adiabatic if a molecule remains in its eigenstate as the field strength, e. g., the laser intensity, is changed. This condition can be fulfilled for most quantum mechanical systems, including non-resonant adiabatic alignment,<sup>39</sup> when the Hamiltonian evolves sufficiently slowly in time. However, in contrast to adiabatic alignment, adiabatic mixed-field orientation tends to be more challenging, because the energy-spacing within the doublets becomes very small inside the laser field.<sup>40,41</sup>

Here, we present a combined experimental and computational investigation of the degree of orientation of rovibronic-ground-state-selected OCS molecules for various laser intensities and dc electric field strengths. The presented experimental setup allows for the use of comparably strong dc electric fields of 20 kV/cm. The experimental findings are compared to the theoretical description obtained by solving the time-dependent Schrödinger equation for the mixed-field orientation of the populated states within the state-selected molecular beam.

## II. METHODS

### A. Experiment

The experimental setup is depicted in Fig. 1. A supersonic molecular beam was generated by expanding a mixture of 500 ppm OCS seeded in 50 bar of helium into vacuum through an Even-Lavie-valve<sup>42</sup> at a repetition rate of 250 Hz. The beam was collimated by two skimmers, 7.4 cm and 23.1 cm downstream from the nozzle. An electrostatic deflector,<sup>37,43</sup> placed 25.9 cm downstream from the nozzle, dispersed the molecular beam according to its quantum states.<sup>31,37</sup> A cross section of the deflector and

<sup>a)</sup> Electronic mail: sebastian.trippel@cfel.de

<sup>b)</sup> Electronic mail: rogonzal@ugr.es

<sup>c)</sup> Electronic mail: jochen.kuepper@cfel.de;

website: <https://www.controlled-molecule-imaging.org>

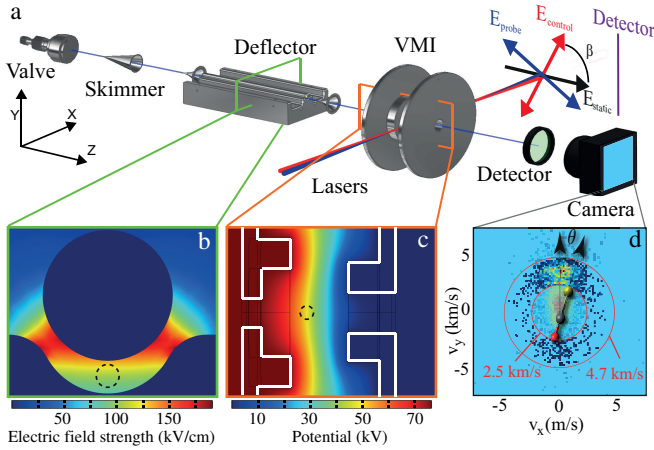


FIG. 1. (Color online) (a) Experimental setup and definition of the axis system and relevant directions and angles.  $\beta$  is the angle between the static electric field and the polarization vector of the control laser pulse; probe and control laser polarization are perpendicular to each other. Colored wireframes mark the positions of the cross sections depicted below. (b) Cross section of the deflector and the corresponding electric field strength. The position of the molecular beam is marked as a black dashed circle. (c) Cross section of the VMI and the corresponding electric potential. The dashed circle marks the interaction region of the molecular beam with the laser pulses and the white frames the electrodes. (d) Typical velocity map of  $S^+$  ions from ionization of oriented OCS.  $\theta_{2D}$  is defined by the angle between the laboratory fixed  $Y$ -axis and the molecule fixed  $z$ -axis projected onto the detector surface. Velocity cuts used in the analysis are illustrated by red circles in the detector image.

its electric field are shown in Fig. 1 b. A third skimmer was positioned 1.4 cm behind the deflector for further differential pumping.

The molecules are oriented and probed inside a velocity map imaging spectrometer (VMI) consisting of two electrodes.<sup>44</sup> The control and probe laser pulses with a central wavelength of 800 nm were provided by an amplified femtosecond laser system.<sup>32</sup> The temporal profile of the control laser pulse had a sawtooth shape with a slow rising edge (600 ps, 2.5-97.5%) and a fast falling edge (250 ps). We measured the spatial beam profile, in intensity, with a beam profiler (SpiriCon SP620U), which yields  $\sigma = 17 \mu\text{m}$  and  $\sigma' = 18 \mu\text{m}$  along the two principal axes of the profile; the first (short) axis is rotated  $17^\circ$  away from the laboratory  $Y$  axis. This resulted in a peak intensity up to  $I_{\text{control}} \approx 6 \times 10^{11} \text{ W/cm}^2$ . The intensity was controlled by a half-wave plate mounted on a rotation stage in combination with a polarization filter. The degree of orientation was probed through Coulomb explosion imaging following multiple ionization of OCS by a 30 fs laser pulse focused down to  $\sigma_1 = 13 \mu\text{m}$ ,  $\sigma_2 = 17 \mu\text{m}$ , which resulted in a peak intensity of  $I_{\text{probe}} \approx 1 \times 10^{14} \text{ W/cm}^2$ . The first principal axis is rotated by  $43^\circ$  towards the laboratory  $Y$  axis. The relative timing between the control and probe laser pulses was varied with a delay stage positioned in the

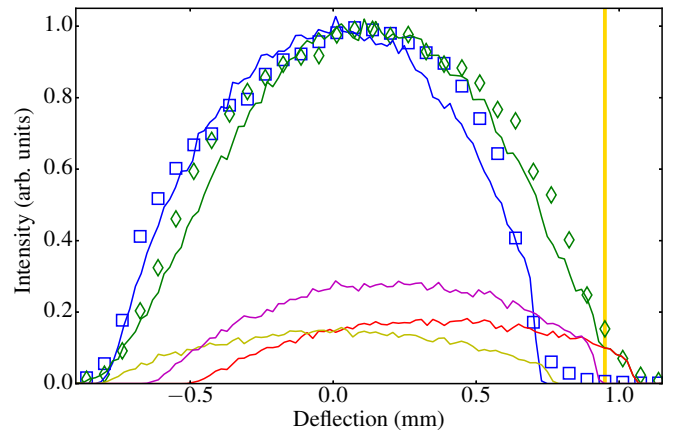


FIG. 2. (Color online) Measured profiles along the laboratory  $Y$ -axis for the deflected (rhombuses) and undeflected (squares) molecular beams. The solid lines represent simulations of the density profile for the deflected  $|0, 0\rangle$ ,  $|1, 0\rangle$ ,  $|1, 1\rangle$  states in red, brown, and purple, respectively and for the sum of these states in green. The blue line is the sum of the undeflected states. The vertical yellow line depicts the position of the laser focus used for the orientation experiments in the molecular beam.

laser beam path of the probe laser. Both laser pulses were linearly polarized with polarization vectors perpendicular to each other. The orientation of both polarization vectors around the laboratory fixed  $X$ -axis, and, therefore, the angle  $\beta$  between the ac and the dc electric fields were simultaneously controlled by a half wave plate. At  $\beta = 35^\circ$  we achieved the best compromise between the strongest orientation, with its maximum at  $\beta = 0^\circ$ , and the ideal detection efficiency, with its maximum at  $\beta = 90^\circ$ . For  $\beta = 35^\circ$ , the component of the dc electric field parallel to the polarization axis of the control laser is reduced to  $\cos(35^\circ) E_{\text{stat}} \approx 0.82 E_{\text{stat}}$ .

The temporal intensity profile of the chirped control laser pulse has been determined as described in appendix A and is shown in Fig. 6 c. For use in computations we applied a Fourier-transform-based low-pass filter to remove frequencies above 81 GHz in the temporal profile of the pulse, which correspond to the limit of the pixel size of the CCD within the spectrometer; the resulting pulse is depicted by the blue area in Fig. 5 a.

The deflection of the molecular beam was characterized by vertically scanning the  $Y$  position of the focus of the probe laser pulse across the molecular beam using a corresponding translation of the focusing lens. The integrated ion signal at each position is proportional to the column density at the corresponding  $Y$  position in the molecular beam. Fig. 2 shows the measured normalized density profiles of the deflected (rhombuses) and the undeflected (squares) molecular beams. The molecules are deflected to positive  $Y$  values by the interaction of their quantum-state-specific dipole moment  $\mu_{\text{eff}}$  with the inhomogeneous electric field. The solid lines represent numerical simulations<sup>37,45</sup> of the density profiles for the undeflected (blue) and deflected (green) molecular beams

as well as the individual contributions to the deflected beam by the  $|J, M\rangle = |0, 0\rangle$ ,  $|1, 0\rangle$ ,  $|1, 1\rangle$  states in red, brown, and purple, respectively. From these simulations we obtain a rotational temperature of 2 K for the original molecular beam; this fairly high temperature<sup>37</sup> is ascribed to the low stagnation pressure and not fully optimized operation conditions of the valve, but is not critical for the investigation performed here. The yellow bar at 0.95 mm in Fig. 2 indicates the position where the orientation experiments were performed. The estimated ground state population at this position was  $0.95 \pm 0.05$ , with the remaining population in the  $|1, 1\rangle$  state.

It was predicted that dc field strengths on the order of  $E_{\text{stat}} = 10 \text{ kV/cm}$  are required to achieve adiabatic orientation with 500 ps pulses.<sup>40</sup> In order to achieve such strong fields a two plate velocity map imaging spectrometer<sup>44</sup> was set up. A sectional view of the electrodes and typical potentials are shown in Fig. 1c. The two-plate design allows for a much stronger field for a given repeller-electrode potential than for the classical three-plate VMI,<sup>46</sup> e.g.,  $E_{\text{stat}} = 20.7 \text{ kV/cm}$  at  $U_r = 80 \text{ kV}$ . In addition, as the magnification of the velocity map scales with  $1/\sqrt{U_r}$ , the measured detector images are larger compared to a classical VMI operated at the same electric field strength. Velocity-focusing conditions were obtained by positioning the laser focus at a specific  $Z$  position between the two electrodes. This position is independent of the applied repeller voltage, which allows for continuous tuning of  $E_{\text{stat}}$  without a change of the VMI focusing conditions.

The velocity maps are detected by a position sensitive detector, a combination of two multi-channel plates (MCPs) in Chevron configuration and a phosphor screen. A CMOS camera (Optronis CL600X2) with a repetition rate of 1 kHz was used to film the screen. The positions of individual ions were determined via a centroiding algorithm.<sup>47</sup> Gating the detector by a fast high-voltage switch (Behlke HTS 31-03-GSM) allowed to distinguish ionic fragments by their time of flight and to record VMIs for individual fragments. Fig. 1d shows a typical  $S^+$ -position histogram. Red circles indicate the area between  $v_{\parallel} = \sqrt{v_x^2 + v_y^2} = 2500 \text{ m/s}$  and  $v_{\parallel} = 4700 \text{ m/s}$ ; this range was used to determine the degree of orientation in all measurements. Ions recorded in this area originate from the Coulomb fragmentation channel  $\text{OCS} + n\gamma \rightarrow \text{OC}^+ + S^+$ , which is a directional fragmentation along the C-S bond of the molecule. Slower fragmentation channels with velocities  $v_{\parallel} < 2500 \text{ m/s}$ , resulting from singly-ionized molecules, are much more intense and not shown.<sup>41</sup> The degree of orientation is characterized by the ratio  $N_{\text{up}}/N_{\text{tot}}$  of  $S^+$  ions hitting the detector on the upper half  $N_{\text{up}}$  divided by the total number of  $S^+$  ions  $N_{\text{tot}}$ .

## B. Theory

To obtain physical insight into the experimental orientation, a theoretical description of the rotational dynamics

of OCS in the experimental field configuration was performed. The dc electric field is always turned on adiabatically, which was computationally checked to be valid for the current experimental parameters, and the adiabatic pendular states of the dc-field configuration were taken as the initial states in these calculations. Then, the time-dependent Schrödinger equation was solved for a constant dc field using the temporal profile of the experimental control laser pulses. To compare with the experimental observations, the theoretical orientation ratio  $N_{\text{up}}/N_{\text{tot}}$  was computed including the volume effect, which took into account the spatial intensity profiles of the control and the probe laser pulses (*vide supra*) and the experimental velocity distribution of the ions after the Coulomb explosion in the range  $2500 \text{ m/s} \leq v_{\parallel} \leq 4700 \text{ m/s}$ .<sup>48</sup> If the mixed-field dynamics was adiabatic, the molecule remained in the same pendular eigenstate as the laser pulse is turned on and the Hamiltonian evolves with time.<sup>38</sup> The rotational dynamics were analyzed by projecting the time-dependent wave function on the basis formed by the adiabatic pendular states, which was obtained by solving the time-independent Schrödinger equation for the instantaneous Hamiltonian at time  $t$ , including both, the interactions with the ac and dc fields. These projections onto the adiabatic pendular basis allowed us to disentangle the field-dressed dynamics for each state of the molecular beam as well as to identify the sources of non-adiabatic effects.

## III. EXPERIMENTAL RESULTS

Fig. 3 shows the experimental degree of orientation  $N_{\text{up}}/N_{\text{tot}}$  as a function of the peak control laser intensity  $I_{\text{control}}$  for experimental dc electric field strengths  $E_{\text{stat}} = 5.2 \text{ kV/cm}$ ,  $10.4 \text{ kV/cm}$ ,  $15.6 \text{ kV/cm}$ , and  $20.7 \text{ kV/cm}$ . A small degree of anti-orientation<sup>49</sup> at zero and weak control laser intensities was observed. This is due to the combined effect of “brute-force” orientation, generated by the static electric field of the VMI spectrometer, and geometric alignment, i.e., selective ionization of OCS by the probe laser, which results in preferred ionization of anti-oriented molecules. For all four electric field strengths, the degree of orientation increased with increasing peak control laser intensity up to  $I_{\text{control}} \approx 1 \times 10^{11} \text{ W/cm}^2$ . The slope of the experimental degree of orientation was the same for  $E_{\text{stat}} = 10.4, 15.6,$  and  $20.7 \text{ kV/cm}$ , while it was slightly lower for  $5.2 \text{ kV/cm}$ . For  $I_{\text{control}} > 2 \times 10^{11} \text{ W/cm}^2$ , the degree of orientation was nearly constant with further increasing laser intensities. In this plateau region the degree of orientation was, within error estimates, independent of the dc field strengths for  $E_{\text{stat}} \geq 10 \text{ kV/cm}$ , while it was reduced for  $5.2 \text{ kV/cm}$ . The inset of Fig. 3 shows the experimental and theoretical mean degree of orientation in the plateau region as a function of the dc field strength. All data points between  $I_{\text{control}} = 3 \times 10^{11} \text{ W/cm}^2$  and  $6.4 \times 10^{11} \text{ W/cm}^2$ , indicated by the blue area in the main

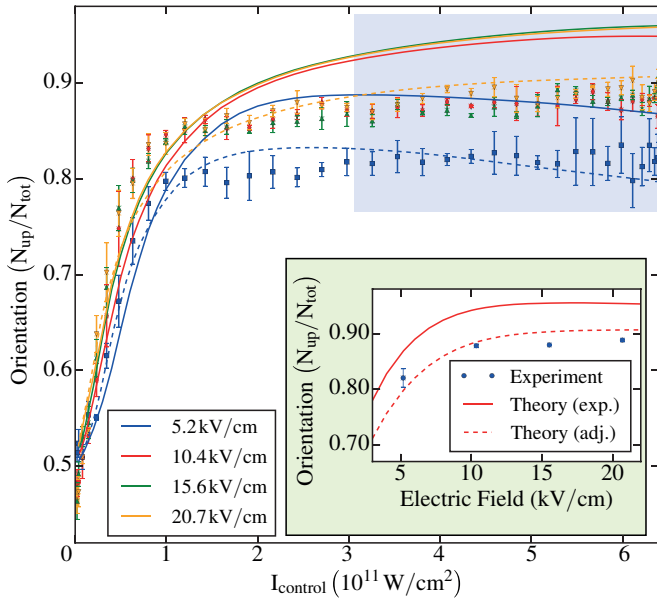


FIG. 3. (Color online) Experimental (points) and theoretical (solid and dashed lines) degree of orientation as a function of the peak control laser intensity for  $\beta = 35^\circ$  and static electric field strengths of 5.2 kV/cm, 10.4 kV/cm, 15.6 kV/cm, and 20.7 kV/cm. In the inset the experimental (points) and theoretical (solid line) mean degree of orientation, averaged over control laser intensities between  $I_{\text{control}} = 3 \times 10^{11} \text{ W/cm}^2$  and  $6.4 \times 10^{11} \text{ W/cm}^2$  (blue area of the main graph), is shown as a function of the dc electric field  $E_{\text{stat}}$ . For the theoretical degree of orientation, depicted by the solid red line, we assumed the populations obtained from the simulated deflection profiles shown in Fig. 2. The dashed line represents calculations with an adjusted population distribution as described in the text.

figure, were taken into account. The experimentally obtained orientation was  $N_{\text{up}}/N_{\text{tot}} = 0.882 \pm 0.004$  for dc field strengths of 10.4 kV/cm and above, indicating nearly adiabatic orientation for the ground state. For 5.2 kV/cm, we had a 7% smaller degree of orientation of  $N_{\text{up}}/N_{\text{tot}} = 0.820$ .

#### IV. DISCUSSION

To understand the saturation of the degree of orientation as a function of the dc field strength the eigenenergies of the adiabatic pendular states of OCS were examined. Fig. 4 a shows the eigenenergies for  $E_{\text{stat}} = 5.2 \text{ kV/cm}$  (dashed lines) and  $20.7 \text{ kV/cm}$  (solid lines) as a function of the control laser intensity.<sup>50</sup> As the laser intensity increases, the two pendular states  $|0, 0, e\rangle_p$  and  $|1, 1, e\rangle_p$  form a near-degenerate doublet; their energy spacing in the strong-ac-field limit is given by  $\Delta E \approx 2\mu_p E_{\text{stat}} \cos \beta$  with the permanent dipole moment  $\mu_p$ . In order to ensure adiabatic orientation, any time scale contained in the temporal envelope of the control laser pulse has to be longer than the time scale that corresponds to the instantaneous energy difference in the laser field. There-

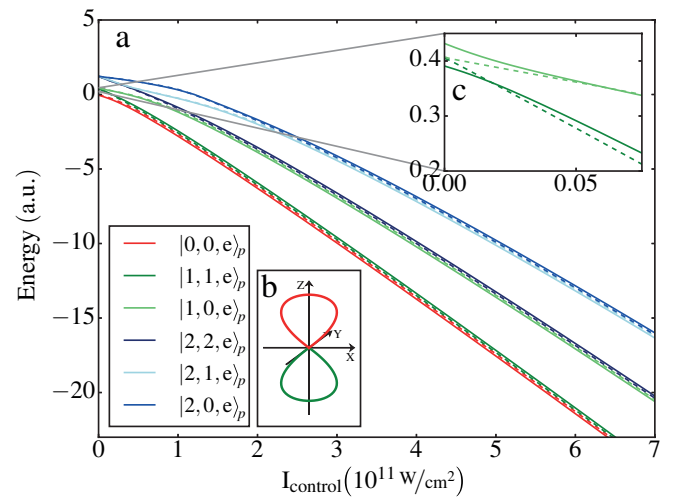


FIG. 4. (Color online) (a) Energy of the  $|0, 0, e\rangle_p$ ,  $|1, 1, e\rangle_p$ ,  $|1, 0, e\rangle_p$ ,  $|2, 2, e\rangle_p$ ,  $|2, 1, e\rangle_p$ , and  $|2, 0, e\rangle_p$  states as a function of the control laser intensity  $I_{\text{probe}}$  for a static electric field strengths with  $E_{\text{stat}} = 5.2 \text{ kV/cm}$  (dashed lines), and  $E_{\text{stat}} = 20.7 \text{ kV/cm}$  (solid lines). (b) Sketch of the square of the  $|0, 0, e\rangle_p$  and  $|1, 1, e\rangle_p$  wave functions at  $E_{\text{stat}} = 20.7 \text{ kV/cm}$ .

fore, e.g., the rise time of the control laser pulse has to be longer for a dc field of  $E_{\text{stat}} = 5.2 \text{ kV/cm}$  than for a dc field of  $20.7 \text{ kV/cm}$ . If this requirement is not fulfilled, the dynamics becomes non-adiabatic and population is transferred between the two pendular states forming the doublet. In this case the resulting orientation for a system starting in the ground state is reduced since the two pendular states orient in opposite directions, see Fig. 4 b. For rotationally excited states, the field-dressed dynamics is more complicated. In addition to the pendular doublet formation, the field-free-degenerate  $|J, M\rangle$  manifold splits into distinct  $M$  components. This results in narrow avoided crossings between energetically neighboring pendular states in the combined field. The avoided crossing between the  $|1, 1, e\rangle_p$  and  $|1, 0, e\rangle_p$  states is shown in Fig. 4 c for  $E_{\text{stat}} = 5.2 \text{ kV/cm}$  (dashed lines) and  $20.7 \text{ kV/cm}$  (solid lines). A larger splitting is observed for stronger dc fields and, therefore, the corresponding dynamics is more adiabatic. Our calculations have shown that a field strength on the order of 400 kV/cm is required to provide adiabatic orientation for the  $J = 1$  states with a control pulse similar to the experimental one, but without roughness.

In Fig. 3 the slopes of all experimentally determined degrees of orientation were steeper than for the calculated ones. A possible reason for this discrepancy are errors in the experimentally determined intensity of the control laser, which relies on a determination of the spatial profile of the laser focus. For these beam-profile measurements, the laser beam had to be attenuated by seven orders of magnitudes, which was achieved by using reflections of optical flats and neutral density filters and which might have affected the beam profile. Furthermore, the profile

of the laser focus might change slightly with pulse energy, for instance, due to self focusing at high pulse energies. The slopes of the experiment and the calculations match nicely if we assume a 1.43 times more intense control laser beam, well within our error estimates.

The theoretical degree of orientation taking into account our experimental conditions are shown as solid lines in Fig. 3. The initial rotational state distribution is given by  $w(|0,0,e\rangle_p) = 0.95$ ,  $w(|1,1,e\rangle_p) = 0.025$ , and  $w(|1,1,o\rangle_p) = 0.025$ , corresponding to the state distribution obtained from the deflection profile in Fig. 2 assuming that the individual states are adiabatically transferred from the deflector to the interaction region inside the velocity map imaging spectrometer. The experimentally determined temporal laser intensity profile, shown in Fig. 5 a, was taken into account. In comparison to the experimental results we observe a higher degree of orientation for the theoretical curves. We attribute this discrepancy to the following effects: First, simulations have shown that molecules in excited rotational states are not adiabatically transferred from the deflector to the velocity map imaging spectrometer. The non adiabatic transfer is mostly caused by rotating electric field vectors<sup>51</sup> in the fringe field regions of the deflector and the VMI. Moreover, Majorana transitions could occur in field free regions. Second, a smoother temporal profile of the laser (*vide supra*) pulse would result in a larger (smaller) weight of the  $|1,1,e\rangle_p$  ( $|1,0,e\rangle_p$ ) state due to a more-adiabatic passage at the corresponding avoided crossing. Because  $|1,1,e\rangle_p$  is anti-oriented while  $|1,0,e\rangle_p$  is oriented this would lead to a decreased degree of orientation.

Adjusting the input parameters for the calculations, a better agreement between experiment and theory was obtained. The dashed lines in Fig. 3 correspond to calculations where the peak intensity was increased by a factor of 1.43 and an initial state population of  $w(|0,0,e\rangle_p) = 0.8$ ,  $w(|1,1,e\rangle_p) = 0.066$ ,  $w(|1,1,o\rangle_p) = 0.066$ , and  $w(|1,0,e\rangle_p) = 0.066$  was assumed. The results of these calculations show a better agreement with the experimental measurements.

The theoretical curve for 5.2 kV/cm shows a decrease of the degree of orientation for increasing laser intensities above  $3 \times 10^{11}$  W/cm<sup>2</sup>. This can be attributed to increased non-adiabatic coupling and population transfer between the  $|0,0,e\rangle_p$  and  $|1,1,e\rangle_p$  states, which gets more important for higher intensities as the slope of the intensity-change and, therefore, the temporal variation of the Hamiltonian gets faster. The theoretical decrease is within the error of the experimental data and is not resolved in the experimental results.

The non adiabatic dynamics can be further investigated by studying the time dependent weights of the decomposition of the time-dependent wave function  $|J,M,s\rangle_t$  in the basis of the adiabatic pendular states  $|J,M,s\rangle_p$ . The purple area in Fig. 5 a depicts the temporal laser beam profile with its slow rising and a fast falling edge obtained from the spectrum of the chirped control laser

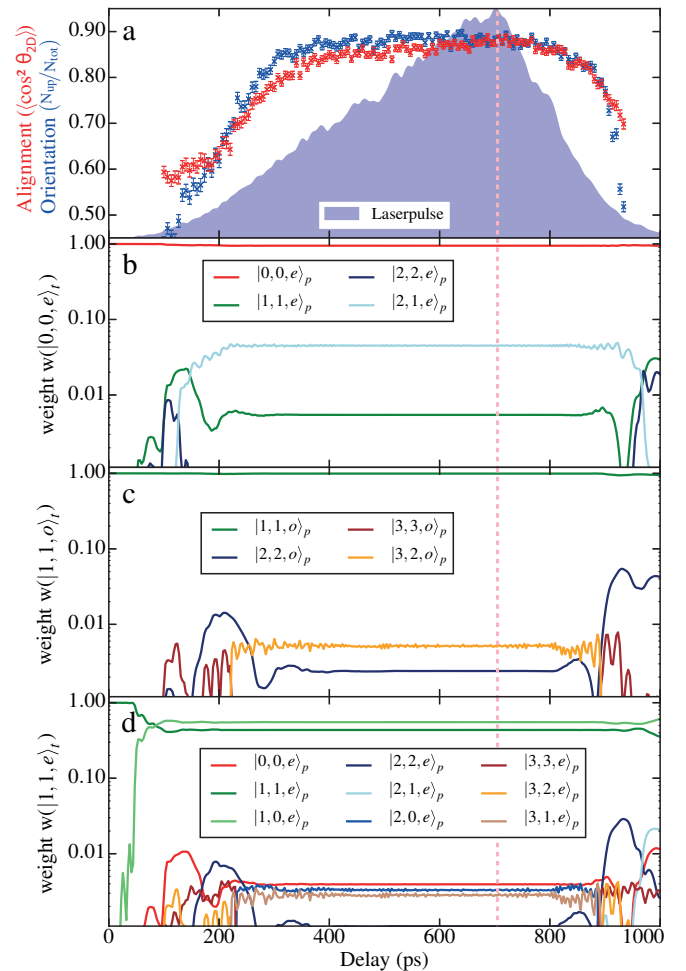


FIG. 5. (Color online) (a) Degree of orientation and alignment as a function of the delay between the control and the probe laser with a peak intensity of the control laser  $I_{\text{control}} = 6 \times 10^{11}$  W/cm<sup>2</sup>, a static electric field of  $E_{\text{stat}} = 20.7$  kV/cm, and a laser polarization direction of  $\beta = 35^\circ$ . The purple area depicts the temporal profile of the control laser. (b, c, d) weights of the basis functions  $|J,M,s\rangle_p$  of the time-dependent wave functions  $|0,0,e\rangle_t$ ,  $|1,1,o\rangle_t$  and  $|1,1,e\rangle_t$ , respectively. The dashed line marks the delay that we used for the measurements shown in Fig. 5

pulse. In addition, the experimental degree of orientation and alignment as a function of the relative timing between the control laser pulse and the probe pulse is shown. The dashed line mark the delay we used for the intensity measurements. Both, the degree of orientation and alignment peak at this intensity. The intensity used for the calculation of the time dependent weights is given by  $6 \times 10^{11}$  W/cm<sup>2</sup>. The dc field strengths is 20.7 kV/cm. In Fig. 5 b-d the time dependent weights  $w$  of systems initially in the  $|0,0,e\rangle_{t=0} = |0,0,e\rangle_p$ ,  $|1,1,o\rangle_{t=0} = |1,1,o\rangle_p$ , and  $|1,1,e\rangle_{t=0} = |1,1,e\rangle_p$  states are presented. A deviation from a weight  $w = 1$  indicates population transfer and, therefore, non-adiabatic dynamics.

The field-dressed dynamics of the ground state  $|0,0,e\rangle_t$

in Fig. 5 b is characterized by the formation of the pendular pair at a delay of approximately 50 ps, when population is transferred to the first rotational excited state resulting in a weight  $w(|1, 1, e\rangle_p) = 5.5 \cdot 10^{-3}$ . In addition, population transfer to states that correlate adiabatically to the  $J = 2$  manifold is observed in the calculation. This is attributed to the roughness of the time-profile and the sudden changes in intensity of the experimental pulse, and not due to the slow 600 ps rise time of the laser pulse, which is long compared to the rotational period of 82 ps. Initially, population is transferred to  $|2, 2, e\rangle_p$ . At stronger ac fields, this state encounters an avoided crossing at which practically all population is diabatically transferred to the  $|2, 1, e\rangle_p$  state. Furthermore, for stronger fields further population transfer from the ground-state pendular doublet proceeds to this  $|2, 1, e\rangle_p$  state, which reaches a population of  $w(|2, 1, e\rangle_p) \approx 4.5 \cdot 10^{-2}$ . Although the field-dressed dynamics of  $|0, 0, e\rangle_t$  including the experimental laser profile is non-adiabatic, the pendular states contributing to the dynamics,  $|0, 0, e\rangle_p$ ,  $|1, 0, e\rangle_p$  and  $|2, 1, e\rangle_p$ , are all strongly oriented and a computed degree of orientation of  $N_{\text{up}}/N_{\text{tot}} = 0.976$  is obtained for  $|0, 0, e\rangle_t$  at the peak laser intensity. We have also performed calculations with an ideal pulse without roughness, which was generated by fitting error functions to the experimental pulse. For this completely smooth theoretical pulse the field-dressed dynamics of the ground-state state is only affected by the formation of the pendular doublet and the dynamics would be completely adiabatic, confirming that the remaining non-adiabaticity is due to the, albeit small, experimental noise in the laser intensity.

For the ground state of the odd irreducible representation,  $|1, 1, o\rangle_t$ , we encounter an equivalent field-dressed dynamics, shown in Fig. 5 c; it is slower because the pendular doublet formation occurs at stronger ac fields. At approximately 100 ps we observe an ac-field-induced population transfer between the initially populated  $|1, 1, o\rangle_p$  state and the  $|3, 3, o\rangle_p$  state. At 200 ps later this population transfers diabatically to the  $|3, 2, o\rangle_p$  state. Almost simultaneously, and due to the formation of the first pendular doublet in this irreducible representation, there is some population transferred from the  $|1, 1, o\rangle_p$  state to  $|2, 2, o\rangle_p$ . At the peak intensity, the pendular states significantly contributing to the time-dependent wave function  $|1, 1, o\rangle_t$  are  $w(|1, 1, o\rangle_p) = 0.993$ ,  $w(|2, 2, o\rangle_p) = 2.4 \cdot 10^{-3}$ , and  $w(|3, 2, o\rangle_p) = 5.2 \cdot 10^{-3}$ . Analogously to the absolute ground-state, the dynamics of this state  $|1, 1, o\rangle_t$  in an ideal pulse would only be affected by the formation of the pendular doublet between the states  $|1, 1, o\rangle_p$  and  $|2, 2, o\rangle_p$ .

In Fig. 5 d the weights of the expansion coefficients of the time-dependent  $|1, 1, e\rangle_t$  wave function for the experimental pulse with peak intensity  $6 \times 10^{11}$  W/cm<sup>2</sup> and a dc field with strength 20.7 kV/cm is presented. The mixed-field dynamics of this state is more complicated. In the presence of a tilted static electric field, the pendular states  $|1, 1, e\rangle_p$  and  $|1, 0, e\rangle_p$  are energetically very close,

and even a weak ac field provokes a strong coupling between them. At weak laser intensities, when the splitting of the  $|1, M, e\rangle_p$  manifold due to the strong dc field takes place, a significant amount of population is transferred between them. Thereafter, the state  $|1, 0, e\rangle_p$  possesses the dominant contribution to the  $|1, 1, e\rangle_t$  state. This non-adiabatic behavior takes place before the pendular doublet formation, i. e., at low intensities and short times. By further increasing the ac field strength, population is transferred to  $|0, 0, e\rangle_p$  and  $|2, 2, e\rangle_p$  due to the formation of the pendular doublets with  $|1, 1, e\rangle_p$  and  $|1, 0, e\rangle_p$ , respectively. Due to ac-field-induced couplings with other pendular states and narrow avoided crossings, we observed that many adiabatic pendular states contribute to the dynamics. At the peak intensity, the pendular states that significantly contribute to the time-dependent wave function  $|1, 1, e\rangle_t$  are  $w(|0, 0, e\rangle_p) = 3.9 \cdot 10^{-3}$ ,  $w(|1, 1, e\rangle_p) = 0.435$ ,  $w(|1, 0, e\rangle_p) = 0.553$ ,  $w(|2, 2, e\rangle_p) = 1.1 \cdot 10^{-3}$ ,  $w(|2, 1, e\rangle_p) = 6 \cdot 10^{-4}$ ,  $w(|2, 0, e\rangle_p) = 3 \cdot 10^{-3}$ ,  $w(|2, 0, e\rangle_p) = 3 \cdot 10^{-3}$ , and  $w(|3, 1, e\rangle_p) = 2.8 \cdot 10^{-3}$ . Since  $|1, 1, e\rangle_p$  is anti-oriented and cancels the contributions from other states,  $|1, 1, e\rangle_t$  shows no orientation at the peak intensity, i. e.,  $N_{\text{up}}/N_{\text{tot}} = 0.50$ . In contrast, the dynamics of this  $|1, 1, e\rangle_t$  state in an ideal pulse without roughness is mainly affected by the splitting of the  $|1, M, e\rangle_p$  manifold, and weakly by the subsequent formation of the pendular pairs. For this ideal pulse, only two adiabatic pendular states contribute significantly, with  $w(|1, 1, e\rangle_p) = 0.652$  and  $w(|1, 0, e\rangle_p) = 0.346$ , resulting in anti-orientation. For the ideal pulse with peak intensity  $6 \times 10^{11}$  W/cm<sup>2</sup> and a dc field of 50 kV/cm, the non-adiabaticity during the splitting of the  $|J, M, e\rangle_p$  manifold would be significantly reduced, and the population-transfer from  $|1, 1, e\rangle_p$  to  $|1, 0, e\rangle_p$  would be  $< 0.011$ .

## V. CONCLUSION

Adiabatic mixed field orientation of ground-state-selected OCS molecules has been demonstrated using strong dc electric fields of 10–20 kV/cm. The experiments demonstrate strong orientation with  $N_{\text{up}}/N_{\text{tot}} = 0.882$  in agreement with our theoretical description. For dc electric fields of 10.4 kV/cm or stronger, the observed degree of orientation was independent of the dc electric field strength, which indicated that the molecules in their ground state are oriented adiabatically. Comparison with calculations showed that only a very small fraction of the population was transferred to excited states. The deviation of the degree of orientation from its maximal possible value of  $N_{\text{up}}/N_{\text{tot}} = 0.976$  was attributed to contributions of excited rotational states present in the deflected part of the molecular beam that was used in the orientation experiments. Preparing the molecules in the absolute ground state would result in full adiabatic orientation dynamics and, therefore, in an even higher degree of orientation. The adiabatic orientation of an excited

rotational state is more challenging. Avoided crossing and the degeneracy at low laser intensity make non-adiabatic behavior more likely.

Compared to other techniques<sup>8,21–24</sup> our approach ensures a strong degree of orientation while employing only moderately strong laser intensities on the order of  $1 \times 10^{11}$  W/cm<sup>2</sup>, which are far below the onset of ionization, even for larger molecules.<sup>52</sup> Moreover, these moderate fields strengths allow for the investigation of chemical dynamics, using molecular-frame-imaging approaches, without significant distortions of the dynamics.

Our findings hold for polar molecules in general, as the Hamiltonian can be rescaled accordingly. Due to the complexity of the rotational level structure of asymmetric tops, non-adiabatic effects will have a larger impact on the orientation dynamics of these more complex molecules.<sup>53,54</sup> Nevertheless, our findings hold for any molecule prepared in the rotational ground state; the experimental realization of such a sample was experimentally demonstrated for C<sub>7</sub>H<sub>5</sub>N using the alternating-gradient  $m/\mu$  selector.<sup>36,55,56</sup>

The improved adiabaticity in mixed field orientation and the resulting increase in the degree of orientation will improve, especially for complex molecules, imaging experiments with fixed-in-space molecules such as the investigation of molecular-frame photoelectron angular distributions<sup>3,57,58</sup> or the recording of molecular movies by x-ray<sup>10</sup> and electron diffraction<sup>9,11</sup> or photoelectron holography.<sup>5,59</sup>

## VI. ACKNOWLEDGEMENTS

Besides DESY, this work has been supported by the *Deutsche Forschungsgemeinschaft* (DFG) through the excellence cluster “The Hamburg Center for Ultrafast Imaging – Structure, Dynamics and Control of Matter at the Atomic Scale” (CUI, EXC1074) and the Helmholtz Association “Initiative and Networking Fund”. R.G.F. gratefully acknowledges financial support by the Spanish project FIS2014-54497-P (MINECO) and the Andalusian research group FQM-207.

### Appendix A: Measurement of the temporal control laser profile

The temporal profiles of the control-laser pulses were deduced from a measurement of their spectrum and a calibrated wavelength-to-time conversion. All spectra were recorded with a commercial spectrometer (Photon Control SPM-002-X). The conversion function between the measured spectrum, shown in Fig. 5 a, and the corresponding temporal intensity profile of the control laser pulse, shown in Fig. 5 d, was determined from the spectral interference of the control laser and the time-delayed 30 fs probe laser pulses. Both laser beams were linearly polarized, parallel to each other, colinearly overlapped,

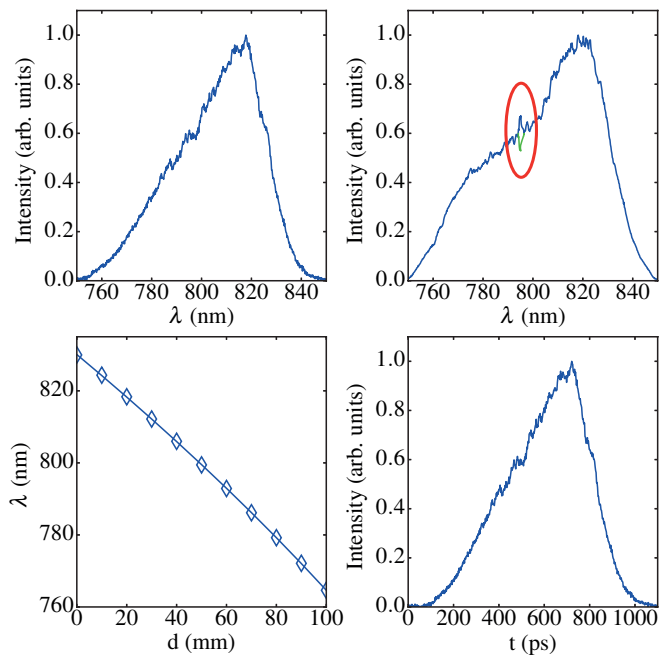


FIG. 6. (Color online) (a) Spectrum of the control laser beam. (b) Interference spectrum of the control and probe laser beam. The red ellipse marks the position of the spectral interference pattern. The green line indicates the amplitude of the interference. (c) Measurement (rhombuses) and quadratic fit (line) of the wavelength of the interference pattern as a function of the delay stage position. (d) Temporal evolution of the control laser beam.

and their simultaneous spectrum recorded. The resulting spectral interference between the two laser pulses manifests itself as a localized large amplitude fluctuation in the spectrum. These fluctuations mark the position “in time” of the short probe pulse within the spectrum of the temporarily stretched – chirped – control laser pulse. As an example, the combined spectrum of both lasers is shown for one relative timing in Fig. 5 b. The position of the spectral interference is highlighted by the red ellipse and the amplitude of its fluctuation is indicated by the green curve. The wavelength  $\lambda$  of the spectral interference pattern in the spectrum as a function of the delay-stage position  $d$  is shown in Fig. 5 c. The blue line is a quadratic fit according to  $\lambda(d) = \lambda_0 + a d + b d^2$  from which we obtained  $\lambda_0 = 829.99$  nm,  $a = -0.57$  nm/mm and  $b = -8.65 \times 10^{-4}$  nm/mm<sup>2</sup>. The conversion from delay stage position  $d$  to time  $t$  is given by  $t = 2d/c$ , where  $c$  is the speed of light. The factor of two is taking into account that the light was traveling back and forth in the translation stage. The resulting temporal profile of the control laser pulse, calculated according to

$$t(\lambda) = 860 \text{ ps} + \frac{2}{c} \left( 698.2 \text{ mm} - 3.41 \frac{\text{mm}}{\text{nm}} \lambda + 3.098 \frac{\text{mm}}{\text{nm}^2} \lambda^2 \right)$$

is shown in Fig. 6 d.

<sup>1</sup>M. Meckel, D. Comtois, D. Zeidler, A. Staudte, D. Pavičić, H. C. Bandulet, H. Pépin, J. C. Kieffer, R. Dörner, D. M. Villeneuve,

- and P. B. Corkum, "Laser-induced electron tunneling and diffraction," *Science* **320**, 1478–1482 (2008).
- <sup>2</sup>C. Z. Bisgaard, O. J. Clarkin, G. Wu, A. M. D. Lee, O. Geßner, C. C. Hayden, and A. Stolow, "Time-resolved molecular frame dynamics of fixed-in-space CS<sub>2</sub> molecules," *Science* **323**, 1464–1468 (2009).
- <sup>3</sup>L. Holmegaard, J. L. Hansen, L. Kalhøj, S. L. Kragh, H. Stapelfeldt, F. Filsinger, J. Küpper, G. Meijer, D. Dimitrovski, M. Abu-samha, C. P. J. Martiny, and L. B. Madsen, "Photoelectron angular distributions from strong-field ionization of oriented molecules," *Nat. Phys.* **6**, 428 (2010), arXiv:1003.4634 [physics].
- <sup>4</sup>F. Kelkensberg, A. Rouzée, W. Siu, G. Gademann, P. Johnsson, M. Lucchini, R. R. Lucchese, and M. J. J. Vrakking, "Xuv ionization of aligned molecules," *Phys. Rev. A* **84**, 051404 (2011).
- <sup>5</sup>R. Boll, D. Anielski, C. Bostedt, J. D. Bozek, L. Christensen, R. Coffee, S. De, P. Decleva, S. W. Epp, B. Erk, L. Foucar, F. Krasniqi, J. Küpper, A. Rouzée, B. Rudek, A. Rudenko, S. Schorb, H. Stapelfeldt, M. Stener, S. Stern, S. Teichert, S. Trippel, M. J. J. Vrakking, J. Ullrich, and D. Rolles, "Femtosecond photoelectron diffraction on laser-aligned molecules: Towards time-resolved imaging of molecular structure," *Phys. Rev. A* **88**, 061402(R) (2013).
- <sup>6</sup>J. Itatani, J. Levesque, D. Zeidler, H. Niikura, H. Pépin, J. C. Kieffer, P. B. Corkum, and D. M. Villeneuve, "Tomographic imaging of molecular orbitals," *Nature* **432**, 867–871 (2004).
- <sup>7</sup>C. Vozzi, M. Negro, F. Calegari, G. Sansone, M. Nisoli, S. De Silvestri, and S. Stagira, "Generalized molecular orbital tomography," *Nat. Phys.* **7**, 822–826 (2011).
- <sup>8</sup>P. M. Kraus, D. Baykusheva, and H. J. Wörner, "Two-pulse field-free orientation reveals anisotropy of molecular shape resonance," *Phys. Rev. Lett.* **113**, 023001 (2014), arXiv:1311.3923 [physics.chem-ph].
- <sup>9</sup>C. J. Hensley, J. Yang, and M. Centurion, "Imaging of isolated molecules with ultrafast electron pulses," *Phys. Rev. Lett.* **109**, 133202 (2012).
- <sup>10</sup>J. Küpper, S. Stern, L. Holmegaard, F. Filsinger, A. Rouzée, A. Rudenko, P. Johnsson, A. V. Martin, M. Adolph, A. Aquila, S. Bajt, A. Barty, C. Bostedt, J. Bozek, C. Caleman, R. Coffee, N. Coppola, T. Delmas, S. Epp, B. Erk, L. Foucar, T. Gorkhovev, L. Gumprecht, A. Hartmann, R. Hartmann, G. Hauser, P. Holl, A. Hömke, N. Kimmel, F. Krasniqi, K.-U. Kühnel, J. Maurer, M. Messerschmidt, R. Moshhammer, C. Reich, B. Rudek, R. Santra, I. Schlichting, C. Schmidt, S. Schorb, J. Schulz, H. Soltau, J. C. H. Spence, D. Starodub, L. Strüder, J. Thøgersen, M. J. J. Vrakking, G. Weidenspointner, T. A. White, C. Wunderer, G. Meijer, J. Ullrich, H. Stapelfeldt, D. Rolles, and H. N. Chapman, "X-ray diffraction from isolated and strongly aligned gas-phase molecules with a free-electron laser," *Phys. Rev. Lett.* **112**, 083002 (2014), arXiv:1307.4577 [physics].
- <sup>11</sup>J. Yang, M. Guehr, T. Vecchione, M. S. Robinson, R. Li, N. Hartmann, X. Shen, R. Coffee, J. Corbett, A. Fry, K. Gaffney, T. Gorkhovev, C. Hast, K. Jobe, I. Makasyuk, A. Reid, J. Robinson, S. Vetter, F. Wang, S. Weathersby, C. Yoneda, M. Centurion, and X. Wang, "Diffractive imaging of a rotational wavepacket in nitrogen molecules with femtosecond megaelectronvolt electron pulses," *Nat. Commun.* **7**, 11232 (2016).
- <sup>12</sup>P. R. Brooks, "Reactions of oriented molecules," *Science* **193**, 11 (1976).
- <sup>13</sup>H. J. Loesch and A. Remscheid, "Brute force in molecular reaction dynamics: A novel technique for measuring steric effects," *J. Chem. Phys.* **93**, 4779 (1990).
- <sup>14</sup>T. P. Rakitzis, A. J. van den Brom, and M. H. M. Janssen, "Directional dynamics in the photodissociation of oriented molecules," *Science* **303**, 1852–1854 (2004).
- <sup>15</sup>S. Stern, L. Holmegaard, F. Filsinger, A. Rouzee, A. Rudenko, P. Johnsson, A. V. Martin, A. Barty, C. Bostedt, J. Bozek, R. Coffee, S. Epp, B. Erk, L. Foucar, R. Hartmann, N. Kimmel, K.-U. Kühnel, J. Maurer, M. Messerschmidt, B. Rudek, D. Starodub, J. Thøgersen, G. Weidenspointner, T. A. White, H. Stapelfeldt, D. Rolles, H. N. Chapman, and J. Küpper, "Toward atomic resolution diffractive imaging of isolated molecules with x-ray free-electron lasers," *Faraday Disc.* **171**, 393 (2014), arXiv:1403.2553 [physics].
- <sup>16</sup>F. Filsinger, G. Meijer, H. Stapelfeldt, H. Chapman, and J. Küpper, "State- and conformer-selected beams of aligned and oriented molecules for ultrafast diffraction studies," *Phys. Chem. Chem. Phys.* **13**, 2076–2087 (2011).
- <sup>17</sup>J. C. H. Spence and R. B. Doak, "Single molecule diffraction," *Phys. Rev. Lett.* **92**, 198102 (2004).
- <sup>18</sup>B. Friedrich and D. R. Herschbach, "Spatial orientation of molecules in strong electric fields and evidence for pendular states," *Nature* **353**, 412–414 (1991).
- <sup>19</sup>P. A. Block, E. J. Bohac, and R. E. Miller, "Spectroscopy of pendular states – the use of molecular complexes in achieving orientation," *Phys. Rev. Lett.* **68**, 1303–1306 (1992).
- <sup>20</sup>A. Slenczka, B. Friedrich, and D. Herschbach, "Pendular alignment of paramagnetic molecules in uniform magnetic fields," *Phys. Rev. Lett.* **72**, 1806–1809 (1994).
- <sup>21</sup>O. Ghafur, A. Rouzee, A. Gijsbertsen, W. K. Siu, S. Stolte, and M. J. J. Vrakking, "Impulsive orientation and alignment of quantum-state-selected NO molecules," *Nat. Phys.* **5**, 289–293 (2009).
- <sup>22</sup>A. Goban, S. Minemoto, and H. Sakai, "Laser-field-free molecular orientation," *Phys. Rev. Lett.* **101**, 013001 (2008).
- <sup>23</sup>M. J. J. Vrakking and S. Stolte, "Coherent control of molecular orientation," *Chem. Phys. Lett.* **271**, 209–215 (1997).
- <sup>24</sup>S. De, I. Znakovskaya, D. Ray, F. Anis, N. G. Johnson, I. A. Bocharova, M. Magrakvelidze, B. D. Esry, C. L. Cocke, I. V. Litvinyuk, and M. F. Kling, "Field-free orientation of CO molecules by femtosecond two-color laser fields," *Phys. Rev. Lett.* **103**, 153002 (2009), arXiv:0907.3250 [physics.chem-ph].
- <sup>25</sup>H. Harde, S. Keiding, and D. Grischkowsky, "THz commensurate echoes – periodic rephasing of molecular-transitions in free-induction decay," *Phys. Rev. Lett.* **66**, 1834–1837 (1991).
- <sup>26</sup>M. Machholm and N. E. Henriksen, "Field-free orientation of molecules," *Phys. Rev. Lett.* **87**, 193001 (2001).
- <sup>27</sup>S. Fleischer, Y. Zhou, R. W. Field, and K. A. Nelson, "Molecular orientation and alignment by intense single-cycle THz pulses," *Phys. Rev. Lett.* **107**, 163603 (2011), arXiv:1105.1635 [physics.chem-ph].
- <sup>28</sup>K. N. Egodapitiya, S. Li, and R. R. Jones, "Terahertz-induced field-free orientation of rotationally excited molecules," *Phys. Rev. Lett.* **112**, 103002 (2014).
- <sup>29</sup>B. Friedrich and D. Herschbach, "Enhanced orientation of polar molecules by combined electrostatic and nonresonant induced dipole forces," *J. Chem. Phys.* **111**, 6157 (1999).
- <sup>30</sup>L. Holmegaard, J. H. Nielsen, I. Nevo, H. Stapelfeldt, F. Filsinger, J. Küpper, and G. Meijer, "Laser-induced alignment and orientation of quantum-state-selected large molecules," *Phys. Rev. Lett.* **102**, 023001 (2009), arXiv:0810.2307 [physics.chem-ph].
- <sup>31</sup>F. Filsinger, J. Küpper, G. Meijer, L. Holmegaard, J. H. Nielsen, I. Nevo, J. L. Hansen, and H. Stapelfeldt, "Quantum-state selection, alignment, and orientation of large molecules using static electric and laser fields," *J. Chem. Phys.* **131**, 064309 (2009), arXiv:0903.5413 [physics].
- <sup>32</sup>S. Trippel, T. Mullins, N. L. M. Müller, J. S. Kienitz, K. Długolecki, and J. Küpper, "Strongly aligned and oriented molecular samples at a kHz repetition rate," *Mol. Phys.* **111**, 1738 (2013), arXiv:1301.1826 [physics.atom-ph].
- <sup>33</sup>O. Stern, "Zur Methode der Molekularstrahlen I," *Z. Phys.* **39**, 751–763 (1926).
- <sup>34</sup>J. Reuss, "State Selection by Nonoptical Methods," in *Atomic and molecular beam methods*, Vol. 1, edited by G. Scoles (Oxford University Press, New York, NY, USA, 1988) Chap. 11, pp. 276–292.
- <sup>35</sup>J. H. Nielsen, P. Simesen, C. Z. Bisgaard, H. Stapelfeldt, F. Filsinger, B. Friedrich, G. Meijer, and J. Küpper, "Stark-selected beam of ground-state OCS molecules characterized by revivals of impulsive alignment," *Phys. Chem. Chem. Phys.* **13**, 18971–18975 (2011), arXiv:1105.2413 [physics].



- <sup>36</sup>S. Putzke, F. Filsinger, H. Haak, J. Küpper, and G. Meijer, “Rotational-state-specific guiding of large molecules,” *Phys. Chem. Chem. Phys.* **13**, 18962 (2011), arXiv:1103.5080 [physics].
- <sup>37</sup>Y.-P. Chang, D. Horke, S. Trippel, and J. Küpper, “Spatially-controlled complex molecules and their applications,” *Int. Rev. Phys. Chem.* **34**, 557–590 (2015), arXiv:1505.05632 [physics].
- <sup>38</sup>M. Born and V. Fock, “Beweis des Adiabatensatzes,” *Z. Phys.* **51**, 165–180 (1928).
- <sup>39</sup>J. Ortigoso, “Quantum adiabatic theorem in light of the Marzlin-Sanders inconsistency,” *Phys. Rev. A* **86**, 032121 (2012), arXiv:1111.5195 [quant-ph].
- <sup>40</sup>J. H. Nielsen, H. Stapelfeldt, J. Küpper, B. Friedrich, J. J. Omiste, and R. González-Férez, “Making the best of mixed-field orientation of polar molecules: A recipe for achieving adiabatic dynamics in an electrostatic field combined with laser pulses,” *Phys. Rev. Lett.* **108**, 193001 (2012), arXiv:1204.2685 [physics.chem-ph].
- <sup>41</sup>S. Trippel, T. Mullins, N. L. M. Müller, J. S. Kienitz, R. González-Férez, and J. Küpper, “Two-state wave packet for strong field-free molecular orientation,” *Phys. Rev. Lett.* **114**, 103003 (2015), arXiv:1409.2836 [physics].
- <sup>42</sup>U. Even, J. Jortner, D. Noy, N. Lavie, and N. Cossart-Magos, “Cooling of large molecules below 1 K and He clusters formation,” *J. Chem. Phys.* **112**, 8068–8071 (2000).
- <sup>43</sup>F. Filsinger, J. Küpper, G. Meijer, J. L. Hansen, J. Maurer, J. H. Nielsen, L. Holmegaard, and H. Stapelfeldt, “Pure samples of individual conformers: the separation of stereo-isomers of complex molecules using electric fields,” *Angew. Chem. Int. Ed.* **48**, 6900–6902 (2009).
- <sup>44</sup>V. Papadakis and T. N. Kitsopoulos, “Slice imaging and velocity mapping using a single field,” *Rev. Sci. Instrum.* **77**, 3101 (2006).
- <sup>45</sup>Y.-P. Chang, F. Filsinger, B. Sartakov, and J. Küpper, “CMIS-TARK: Python package for the stark-effect calculation and symmetry classification of linear, symmetric and asymmetric top wavefunctions in dc electric fields,” *Comp. Phys. Comm.* **185**, 339–49 (2014), arXiv:1308.4076 [physics].
- <sup>46</sup>A. T. J. B. Eppink and D. H. Parker, “Velocity map imaging of ions and electrons using electrostatic lenses: Application in photoelectron and photofragment ion imaging of molecular oxygen,” *Rev. Sci. Instrum.* **68**, 3477–3484 (1997).
- <sup>47</sup>R. Wester, F. Albrecht, M. Grieser, L. Knoll, R. Repnow, D. Schwalm, A. Wolf, A. Baer, J. Levin, Z. Vager, and D. Zajfman, “Coulomb explosion imaging at the heavy ion storage ring tsr,” *Nuc. Instrum. & Meth. Phys. A* **413**, 379–396 (1998).
- <sup>48</sup>J. J. Omiste, M. Gaerttner, P. Schmelcher, R. González-Férez, L. Holmegaard, J. H. Nielsen, H. Stapelfeldt, and J. Küpper, “Theoretical description of adiabatic laser alignment and mixed-field orientation: the need for a non-adiabatic model,” *Phys. Chem. Chem. Phys.* **13**, 18815–18824 (2011), arXiv:1105.0534 [physics].
- <sup>49</sup>For an anti-oriented state, it holds that  $-1 \leq \langle \cos\theta_{2D} \rangle < 0$  and  $0 \leq N_{up}/N_{tot} < 0.5$ .
- <sup>50</sup>The adiabatic pendular states  $|J, M, s\rangle_p$  are labeled by the quantum numbers  $J$  and  $M = |m_J|$  of the adiabatically correlated field-free rotor states  $|J, M\rangle$  and the symmetry  $s$  with respect to reflection at the plane defined by the dc and ac electric field vectors, denoted  $e$  for even and  $o$  for odd. For the adiabatic following, we take into account that the dc field is turned on first. Once the maximum dc electric field strength is achieved, the ac laser pulse is turned on. These adiabatic-pendular-state labels are amended by a subscript  $p$ .
- <sup>51</sup>T. E. Wall, S. K. Tokunaga, E. a. Hinds, and M. R. Tarbutt, “Nonadiabatic transitions in a Stark decelerator,” *Phys. Rev. A* **81**, 033414 (2010).
- <sup>52</sup>J. Strohaber, T. Mohamed, N. Hart, F. Zhu, R. Nava, F. Pham, A. A. Kolomenskii, H. Schroeder, G. G. Paulus, and H. A. Schuessler, “Intensity-resolved ionization yields of aniline with femtosecond laser pulses,” *Phys. Rev. A* **84**, 063414 (2011).
- <sup>53</sup>J. J. Omiste and R. González-Férez, “Rotational dynamics of an asymmetric-top molecule in parallel electric and nonresonant laser fields,” *Phys. Rev. A* , 033416 (2013).
- <sup>54</sup>J. J. Omiste, R. González-Férez, and P. Schmelcher, “Rotational spectrum of asymmetric top molecules in combined static and laser fields,” *J. Chem. Phys.* **135**, 064310 (2011), arXiv:1106.1586 [physics.chem-ph].
- <sup>55</sup>F. Filsinger, U. Erlekam, G. von Helden, J. Küpper, and G. Meijer, “Selector for structural isomers of neutral molecules,” *Phys. Rev. Lett.* **100**, 133003 (2008), arXiv:0802.2795 [physics].
- <sup>56</sup>F. Filsinger, S. Putzke, H. Haak, G. Meijer, and J. Küpper, “Optimizing the resolution of the alternating-gradient  $m/\mu$  selector,” *Phys. Rev. A* **82**, 052513 (2010).
- <sup>57</sup>M. G. Pullen, B. Wolter, A.-T. Le, M. Baudisch, M. Hemmer, A. Senftleben, C. D. Schroter, J. Ullrich, R. Moshhammer, C. D. Lin, and J. Biegert, “Imaging an aligned polyatomic molecule with laser-induced electron diffraction,” *Nat. Commun.* **6**, 7262 (2015).
- <sup>58</sup>D. Zeidler, A. Staudte, A. B. Bardon, D. M. Villeneuve, R. Dörner, and P. B. Corkum, “Controlling attosecond double ionization dynamics via molecular alignment,” *Phys. Rev. Lett.* **95**, 203003 (2005).
- <sup>59</sup>R. Boll, A. Rouzée, M. Adolph, D. Anielski, A. Aquila, S. Bari, C. Bomme, C. Bostedt, J. D. Bozek, H. N. Chapman, L. Christensen, R. Coffee, N. Coppola, S. De, P. Decleva, S. W. Epp, B. Erk, F. Filsinger, L. Foucar, T. Gorkhover, L. Gumprecht, A. Hömke, L. Holmegaard, P. Johnsson, J. S. Kienitz, T. Kierspel, F. Krasniqi, K.-U. Kühnel, J. Maurer, M. Messerschmidt, R. Moshhammer, N. L. M. Müller, B. Rudek, E. Savelyev, I. Schlichting, C. Schmidt, F. Scholz, S. Schorb, J. Schulz, J. Seltmann, M. Stener, S. Stern, S. Techert, J. Thøgersen, S. Trippel, J. Viehhaus, M. Vrakking, H. Stapelfeldt, J. Küpper, J. Ullrich, A. Rudenko, and D. Rolles, “Imaging molecular structure through femtosecond photoelectron diffraction on aligned and oriented gas-phase molecules,” *Faraday Disc.* **171**, 57–80 (2014), arXiv:1407.7782.